Journal of Telecommunication, Electronic and Computer Engineering
ISSN: 2180 – 1843 e-ISSN: 2289-8131 Vol. 15 No. 2
jtec.utem.edu.my

A New 8D Lorenz-like Hyperchaotic System: Computer Modelling, Circuit Design and Arduino Uno Board Implementation

M.Kopp[1], A. Kopp[2]
[1]*Institute for Single Crystals, NAS Ukraine, Kharkiv, Ukraine*
[2]*National Technical University "Kharkiv Polytechnic Institute", Kyrpychova str. 2, Kharkiv, 61002, Ukraine*
michaelkopp0165@gmail.com

Article Info

Article history:
Received Feb 14th, 2023
Revised Apr 17th, 2023
Accepted May 10th, 2023

Index Terms:
Chaotic behavior
Chaos generator
Computer simulation
Circuit design

Abstract

This paper presents the construction of Matlab-Simulink and LabView models for a novel nonlinear dynamic system of equations in an eight-dimensional (8D) phase space. The Lyapunov exponent spectrum and Kaplan-York dimension were calculated with fixed parameters of the 8D dynamical system. The presence of two positive Lyapunov exponents indicates hyperchaotic behavior. The fractional Kaplan-York dimension shows the fractal structure of strange attractors. An adaptive controller was used to stabilize the 8D chaotic system with unknown system parameters, and an active control method was derived to achieve global chaotic synchronization of two identical 8D chaotic systems with unknown system parameters. Using the results from Matlab-Simulink and LabView models, a chaotic signal generator for the 8D chaotic system was implemented in the Multisim environment. The simulation results of chaotic behavior in the Multisim environment demonstrate similar behavior compared to simulation results from Matlab-Simulink and LabView models. To visualize the new 8D chaotic system, we employed an Arduino Uno board along with eight light-emitting diodes (LEDs). Furthermore, we demonstrated the capability to simulate the new 8D chaotic system in the Proteus 8 environment using the Arduino Uno microcontroller. This advancement in the understanding and implementation of chaotic systems opens doors to numerous possibilities in the realm of secure communication and control systems.

I. INTRODUCTION

Deterministic chaos is now increasingly applied in solving various engineering problems, particulary those related to the design of telecommunication systems [1, 2]. Recent advancements have enabled the physical modeling of nonlinear dynamic equations through the deployment of electronic circuits to create new chaos generators. These generators provide a viable alternative to numerical modeling. One of the most commonly studied dynamical systems that exhibits chaotic behavior is the Lorentz system [3], which is used to describe free convection in an atmosphere. An electronic circuit to generate chaotic signals that behaves similarly to those predicted by numerical experiments based on Lorentz equations was crafted in [4]. The authors of [4] demonstrated an approach to secure data exchange using synchronized chaotic systems, implemented via the Lorenz system in both the transmitter and receiver. This unique modulation process involves the addition of a chaotic masking signal to the information message at the transmitter, and subsequently, the message is retrieved during the demodulation process by deducting the chaotic signal produced in the receiver.

The increasing interest in applying chaotic dynamics for engineering purposes is noteworthy. The study in [4] stimulated the development of electronic chaos generators based on a variety of equations, such as the Rössler equations [5,6], Rikitake equations [7], modified Lorentz equations [8], and Rucklidge equations [9]. More recently, systems producing hyperchaotic oscillations have been developed, such as the Liu systems [10,11], Chen systems [12], and new modifications of the Lorentz equations [13,14] and Rikitake equations [15,16].

This paper focuses on the nonlinear 8D dynamic equationa that describe convection in a non-uniformly rotating electrically conductive fluid in a helical magnetic field [17]. These equations were derived in a similar manner to the Lorentz equations [3], utilizing a minimum order of the Fourier series to represent physical fields. Unlike the the 3D Lorentz equations, these equations resulted in a higher phase space dimension nonlinear dynamic system of equation (8D). Chaotic systems with attractor dimensions greater than 3D offer broader practical applications, particularly in secure communication where high-dimensional chaotic systems are preferred. These systems, due to the presence of more than one Lyapunov exponent, exhibit complex dynamics, thereby increasing the security of information transmission. Given these traits, high-

dimensional chaotic systems are highly suitable for secure information transmission. Therefore, the computer simulation of chaotic signals and the exploration of circuit implementation strategies for chaotic oscillation generators represent critical challenge that warrant investigation.

The aim of this paper is to create computer models of an 8D chaotic dynamic system leveraging the capabilities of the Matlab-Simulink environment and LabView software. To actualize the circuit of the newly developed chaos generator circuit, we employ the NI Multisim package. This software allows us to illustrate the chaotic dynamics through signal oscillograms and attractor phase portraits. Moreover, this study emcompasses a practical implemention of a new 8D chaotic system using the Arduino Uno board.

II. BASIC EQUATIONS OF THE 8D CHAOTIC SYSTEM

According to [17], the dynamic system of equations that describes weakly non-linear convection in an electrically conductive fluid with non-uniform rotation within a helical magnetic field can be expressed as follows:

$$\begin{cases} \dot{X} = -X + RY - TV - HU + \tilde{H}\tilde{W} \\ \dot{V} = -V + HW + \sqrt{Ta}(1+Ro)X \\ \dot{\tilde{V}} = -\tilde{V} + \tilde{\xi}H(1+Rb)U - H\tilde{W} \\ \dot{U} = -Pm^{-1}U + Pr^{-1}X \\ \dot{W} = -Pm^{-1}W - Pr^{-1}V + Ro\sqrt{Ta}U \\ \dot{\tilde{W}} = -Pm^{-1}\tilde{W} + Pr^{-1}\tilde{V} + \tilde{\xi}Pr^{-1}RbX \\ \dot{Y} = Pr^{-1}(-Y + X - XZ) \\ \dot{Z} = Pr^{-1}(-bZ + XY) \end{cases} \quad (1)$$

Equation (1) describes a dynamic system, where the dot over the symbol signifies differentiation with respect to time t. The variables $X, V, \tilde{V}$, $U, W, \tilde{W}$, and Y, Z represent the amplitudes of disturbances in velocity, magnetic fields and temperature fields respectively. The parameters $H, \tilde{H}, Ta, T, Pm, Pr, Ro, \tilde{\xi}, b$ and R are real constants, while Ra (the Rayleigh number) is a bifurcation parameter. The last two equations of system (1) are comparable to the equations found in the Lorentz system [3], which also exhibit chaotic behavior. Thus, the nonlinear system of equations (1) falls within the category of Lorentz-type equations in an eight-dimensional phase space (8D). In a specific case where there is only a constant external axial magnetic field, equations (1) reduce to the six-dimensional Lorentz equations, which were numerically analyzed in [18]. The trajectory in the 8D-dimensional phase space, as described by the nonlinear system of equations (1) is dependent on an extensive range of dimensionless parameters, specifically 11 parameters represented by $H, \tilde{H}, Ta, T, Pm, Pr, Ro, \tilde{\xi}, b$.

Additionally, system (1) exhibits hyperchaotic behaviour with two positive Lyapunov exponents, making it appropriate for secure communication applications. The fractal structure of the attractors is indicated by the fractional Kaplan-York dimension. Moreover, system (1) can be stabilised using an adaptive controller and global chaotic synchronisation of two identical systems can be achieved using an active control method. The properties make system (1) a promising candidate for various applications in chaos-based secure communication and control systems. Using the values of the parameters

$$\begin{aligned} &H = 2, Ta = 1080, T = 0.1, Pm = 1, Pr = 10, b = 8/3, \\ &\tilde{H} = 0.06, \tilde{\xi} = 9.4, Rb = 1/2, Ro = -3/4 \end{aligned} \quad (2)$$

we write system (1) in a form more convenient for modeling:

$$\begin{cases} \dot{x}_1 = -x_1 + Rx_2 - 2x_4 - 0.1x_5 \\ \dot{x}_2 = \frac{1}{10}(-x_2 + x_1 - x_1x_3) \\ \dot{x}_3 = \frac{1}{10}\left(-\frac{8}{3}x_3 + x_1x_2\right) \\ \dot{x}_4 = -x_4 + \frac{1}{10}x_1 \\ \dot{x}_5 = -x_5 + 8.21x_1 + 2x_6 \\ \dot{x}_6 = -x_6 - 24.65x_4 - \frac{1}{10}x_5 \\ \dot{x}_7 = -x_7 + 28.2x_4 - 2x_8 \\ \dot{x}_8 = -x_8 + 0.47x_1 + \frac{1}{10}x_7 \end{cases} \quad (3)$$

In this scenario, new variables were introduced: $x_1 = X, x_2 = Y, x_3 = Z, x_4 = U, x_5 = V, x_6 = W, x_7 = \tilde{V}, x_8 = \tilde{W}$. Subsequently, equations (3) are supplemented with the initial conditions: $x_1(0) = x_2(0) = x_3(0) = x_4(0) = x_5(0) = x_6(0) = x_7(0) = x_8(0) = 1$. Equations (3) contain a singular parameter R, whose changes allow for the exploration of a one-parameter set of solutions. To study the chaotic behaviour of system (3), various numerical methods can be employed.These include the Euler method, the Runge-Kutta method, or the fourth-order Adams-Bashforth method. Additionally, one can calculate the Lyapunov exponents, which serve as a measure to quantify the degree of chaos in the system, and the Kaplan-Yorke dimension, which characterizes the fractal structure of the strange attractor. In addition to numerical simulations, it is also possible to investigate the stability of the system and its synchronization properties, which are important for potential applications in secure communication. Finally, a chaotic signal generator can be designed based on system (3) for experimental verification of its chaotic properties. Furthermore, we aim to examine the chaotic behaviour of system (3) particularly tfor the value of $R = 58$.

III. LYAPUNOV EXPONENTS AND KAPLAN-YORKE DIMENSION

One of the important criteria characterizing the chaotic behavior of a nonlinear dynamical system is the spectrum of Lyapunov exponents. The maximum Lyapunov exponent is a measure of the rate of separation between initially close trajectories in the phase space of a chaotic system. The Benettin algorithm [19,20] is a widely used method for the numerical computing of Lyapunov exponents. In this work, the maximum Lyapunov exponent $L_{max} = 0.0974135$ was calculated for system (3) at a specific parameter value of

$R = 58$. This was carried out following the approach described in [21]. Then, all all Lyapunov exponents were determined more accurately using the Gram-Schmidt orthogonalization.

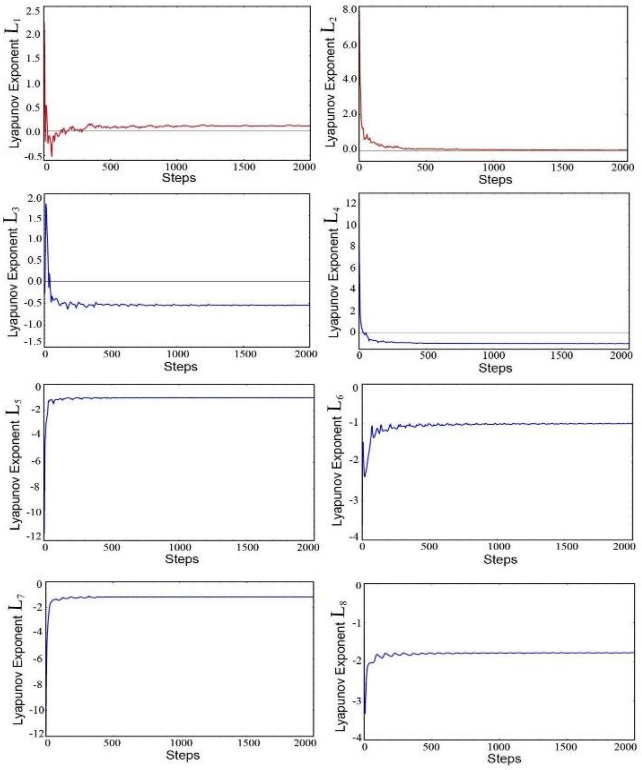

$$L_1 = 0.0914666,\ L_2 = 0.0232093,\ L_3 = -0.549477,$$
$$L_4 = -0.983332,\ L_5 = -1.01154,\ L_6 = -1.01105, \quad (4)$$
$$L_7 = -1.15546,\ L_8 = -1.77049$$

Figure 1: Convergence plot of the Lyapunov spectrum for the system (3).

As shown in Figure 1, the spectrum of Lyapunov exponents (4) has two positive terms L_1, L_2; therefore, system (3) shows hyperchaotic behavior. The maximum Lyapunov exponent of the new hyperchaotic system (3) corresponds to the value $L_{1max} = 0.0914666$.

The sum of the Lyapunov exponents in (4) is negative $L_1 + L_2 + L_3 + L_4 + L_5 + L_6 = -6.36667 < 0$, indicating that the hyperchaotic system (3) is dissipative. The Kaplan-York dimension of the new hyperchaotic system (3) is calculated as

$$D_{KY} = 2 + \frac{L_1 + L_2}{|L_3|} \approx 2.20184 \quad (5)$$

This shows the high complexity of system (3). Figure 1 depicts the dynamics of the Lyapunov exponents of the hyperchaotic system (3).

IV. ADAPTIVE CONTROL OF THE 8D CHAOTIC SYSTEM

In this section, we consider an adaptive controller to stabilize the chaotic system (3) with an unknown system parameter. We represent system (3) in the following form:

$$\begin{cases} \dot{x}_1 = -x_1 + Rx_2 - 2x_4 - 0.1x_5 + u_1 \\ \dot{x}_2 = \frac{1}{10}(-x_2 + x_1 - x_1x_3) + u_2 \\ \dot{x}_3 = \frac{1}{10}\left(-\frac{8}{3}x_3 + x_1x_2\right) + u_3 \\ \dot{x}_4 = -x_4 + \frac{1}{10}x_1 + u_4 \\ \dot{x}_5 = -x_5 + 8.21x_1 + 2x_6 + u_5 \\ \dot{x}_6 = -x_6 - 24.65x_4 - \frac{1}{10}x_5 + u_6 \\ \dot{x}_7 = -x_7 + 28.2x_4 - 2x_8 + u_7 \\ \dot{x}_8 = -x_8 + 0.47x_1 + \frac{1}{10}x_7 + u_8 \end{cases} \quad (6)$$

where $u_1, u_2, u_3, u_4, u_5, u_6, u_7, u_8$ are adaptive controls to be determined using estimate $R(t)$ for the unknown parameter R. We consider the adaptive feedback control law

$$\begin{cases} u_1 = x_1 - R(t)x_2 + 2x_4 + 0.1x_5 - k_1x_1 \\ u_2 = \frac{1}{10}(x_2 - x_1 + x_1x_3) - k_2x_2 \\ u_3 = \frac{1}{10}\left(\frac{8}{3}x_3 - x_1x_2\right) - k_3x_3 \\ u_4 = x_4 - \frac{1}{10}x_1 - k_4x_4 \\ u_5 = x_5 - 8.21x_1 - 2x_6 - k_5x_5 \\ u_6 = x_6 + 24.65x_4 + \frac{1}{10}x_5 - k_6x_6 \\ u_7 = x_7 - 28.2x_4 + 2x_8 - k_7x_7 \\ u_8 = x_8 - 0.47x_1 - \frac{1}{10}x_7 - k_8x_8 \end{cases} \quad (7)$$

In (7), $k_1, k_2, k_3, k_4, k_5, k_6, k_7, k_8$ are positive constants. $R(t)$ is an estimate for the unknown system parameter R. Upon substituting (7) into (6), we obtain:

$$\begin{cases} \dot{x}_1 = (R - R(t))x_2 - k_1x_1 \\ \dot{x}_2 = -k_2x_2 \\ \dot{x}_3 = -k_3x_3 \\ \dot{x}_4 = -k_4x_4 \\ \dot{x}_5 = -k_5x_5 \\ \dot{x}_6 = -k_6x_6 \\ \dot{x}_7 = -k_7x_7 \\ \dot{x}_8 = -k_8x_8 \end{cases} \quad (8)$$

Then, the parameter estimation error is defined by $e = R - R(t)$. After differentiating e with respect to t, we get

$$\frac{de}{dt} = -\frac{dR(t)}{dt} \quad (9)$$

Employing adaptive control theory, we define Lyapunov function as:

$$\Lambda = \frac{1}{2}(x_1^2 + x_2^2 + x_3^2 + x_4^2 + x_5^2 + x_6^2 + x_7^2 + x_8^2 + e^2) \tag{10}$$

It is obvious that V is a positive definite function. Differentiating V from (10), we can obtain:

$$\frac{d\Lambda}{dt} = e\left(x_1 x_2 - \frac{dR(t)}{dt}\right) - k_i^2 x_i^2, (i = 1,2,3,4,5,6,7,8) \tag{11}$$

From (11), we obtain the parameter update law as:

$$\frac{dR(t)}{dt} = x_1 x_2 \tag{12}$$

Therefore, the adaptive control law (7) and the parameter update law (12) can globally and exponentially stabilize the 8D chaotic system (3) with unknown system parameter R for all initial conditions.

V. ADAPTIVE SYNCHRONIZATION OF THE IDENTICAL 8D CHAOTIC SYSTEM

The adaptive synchronization of identical 8D chaotic systems was examined with an unknown system parameter R. For the drive system, system (3) was selected and for the response system, the following system was used.

$$\begin{cases} \dot{y}_1 = -y_1 + Ry_2 - 2y_4 - 0.1y_5 + u_1 \\ \dot{y}_2 = \frac{1}{10}(-y_2 + y_1 - y_1 y_3) + u_2 \\ \dot{y}_3 = \frac{1}{10}\left(-\frac{8}{3}y_3 + y_1 y_2\right) + u_3 \\ \dot{y}_4 = -y_4 + \frac{1}{10}y_1 + u_4 \\ \dot{y}_5 = -y_5 + 8.21y_1 + 2y_6 + u_5 \\ \dot{y}_6 = -y_6 - 24.65y_4 - \frac{1}{10}y_5 + u_6 \\ \dot{y}_7 = -y_7 + 28.2y_4 - 2y_8 + u_7 \\ \dot{y}_8 = -y_8 + 0.47y_1 + \frac{1}{10}y_7 + u_8 \end{cases} \tag{13}$$

where $y_1, y_2, y_3, y_4, y_5, y_6, y_7, y_8$ are the states and $u_1, u_2, u_3, u_4, u_5, u_6, u_7, u_8$ are the controllers to be designed to achieve global chaos synchronization between systems (3) and (13). The synchronization error between the identical chaotic systems is defined as $\xi_i = y_i(t) - x_i(t)$, $(i = 1,2,3,4,5,6,7,8)$.

$$\begin{cases} \dot{\xi}_1 = -\xi_1 + R\xi_2 - 2\xi_4 - 0.1\xi_5 + u_1 \\ \dot{\xi}_2 = \frac{1}{10}(-\xi_2 + \xi_1 - (y_1 y_3 - x_1 x_3)) + u_2 \\ \dot{\xi}_3 = \frac{1}{10}\left(-\frac{8}{3}\xi_3 + (y_1 y_2 - x_1 x_2)\right) + u_3 \\ \dot{\xi}_4 = -\xi_4 + \frac{1}{10}\xi_1 + u_4 \\ \dot{\xi}_5 = -\xi_5 + 8.21\xi_1 + 2\xi_6 + u_5 \\ \dot{\xi}_6 = -\xi_6 - 24.65\xi_4 - \frac{1}{10}\xi_5 + u_6 \\ \dot{\xi}_7 = -\xi_7 + 28.2\xi_4 - 2\xi_8 + u_7 \\ \dot{\xi}_8 = -\xi_8 + 0.47\xi_1 + \frac{1}{10}\xi_7 + u_8 \end{cases} \tag{14}$$

The adaptive control law was written as:

$$\begin{cases} u_1 = \xi_1 - R(t)\xi_2 + 2\xi_4 + 0.1\xi_5 - k_1\xi_1 \\ u_2 = \frac{1}{10}(\xi_2 - \xi_1 + (y_1 y_3 - x_1 x_3)) - k_2\xi_2 \\ u_3 = \frac{1}{10}\left(\frac{8}{3}\xi_3 - (y_1 y_2 - x_1 x_2)\right) - k_3\xi_3 \\ u_4 = \xi_4 - \frac{1}{10}\xi_1 - k_4\xi_4 \\ u_5 = \xi_5 - 8.21\xi_1 - 2\xi_6 - k_5\xi_5 \\ u_6 = \xi_6 + 24.65\xi_4 + \frac{1}{10}\xi_5 - k_6\xi_6 \\ u_7 = \xi_7 - 28.2\xi_4 + 2\xi_8 - k_7\xi_7 \\ u_8 = \xi_8 - 0.47\xi_1 - \frac{1}{10}\xi_7 - k_8\xi_8 \end{cases} \tag{15}$$

where $k_1, k_2, k_3, k_4, k_5, k_6, k_7, k_8$ are positive constants controlling the synchronization speed, $R(t)$ is the estimate of the unknown parameter R.

The parameter estimation error is defined by $e_R = R - R(t)$. As a result, the error dynamics was obtained:

$$\begin{cases} \dot{\xi}_1 = (R - R(t))\xi_2 - k_1\xi_1 \\ \dot{\xi}_2 = -k_2\xi_2 \\ \dot{\xi}_3 = -k_3\xi_3 \\ \dot{\xi}_4 = -k_4\xi_4 \\ \dot{\xi}_5 = -k_5\xi_5 \\ \dot{\xi}_6 = -k_6\xi_6 \\ \dot{\xi}_7 = -k_7\xi_7 \\ \dot{\xi}_8 = -k_8\xi_8 \end{cases} \tag{16}$$

Next, the quadratic Lyapunov function is defined as:

$$\Lambda = \frac{1}{2}(\xi_1^2 + \xi_2^2 + \xi_3^2 + \xi_4^2 + \xi_5^2 + \xi_6^2 + \xi_7^2 + \xi_8^2 + e_R^2) \tag{17}$$

Taking into account that $\dot{e}_R = -dR(t)/dt$, it is found that

$$\frac{d\Lambda}{dt} = \left(\xi_1\xi_2 - \frac{dR(t)}{dt}\right)e_R - k_i\xi_i^2,\ (i = 1,2,3,4,5,6,7,8) \qquad (18)$$

From (18), the parameter update law is obtained as:

$$\frac{dR(t)}{dt} = \xi_1\xi_2 \qquad (19)$$

Thus, the adaptive synchronization of two identical 8D chaotic systems with an unknown system parameter is achieved using the proposed adaptive control law (15) and parameter update law (19). The stability of the synchronized system is guaranteed by Lyapunov's stability theory, where a positive definite function Λ and a negative function $d\Lambda/dt < 0$ are used to ensure asymptotic stability at the origin of the equilibrium state. Consequently, the error between the drive and response systems decreases exponentially $e_R \to 0$ over time $t \to \infty$.

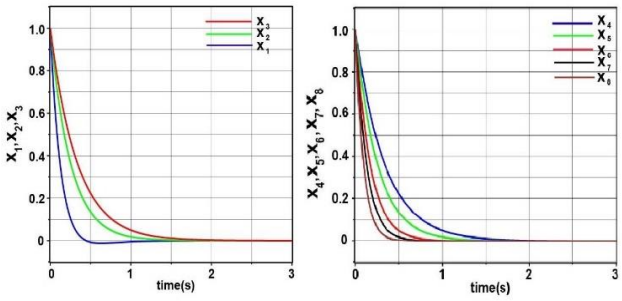

Figure 2: Time history of the controlled chaotic system.

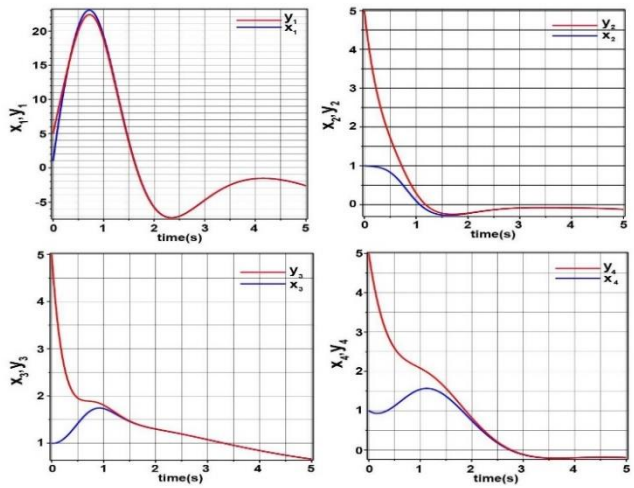

Figure 3: Synchronization of the states $x_1 - y_1, x_2 - y_2, x_3 - y_3, x_4 - y_4$ of the chaotic systems.

VI. RESULTS AND DISCUSSION

For the numerical simulations, the fourth-order Runge-Kutta method is used to solve the novel system (6). The bifurcation parameter value of the novel chaotic system (6) is taken as in the chaotic case, i. e. $R = 58$. The control gains are chosen as $k_1 = 7$, $k_2 = 4$, $k_3 = 3$, $k_4 = 3$, $k_5 = 4$, $k_6 = 6$, $k_7 = 8$, and $k_8 = 11$. The initial values of the chaotic system (6) are taken as

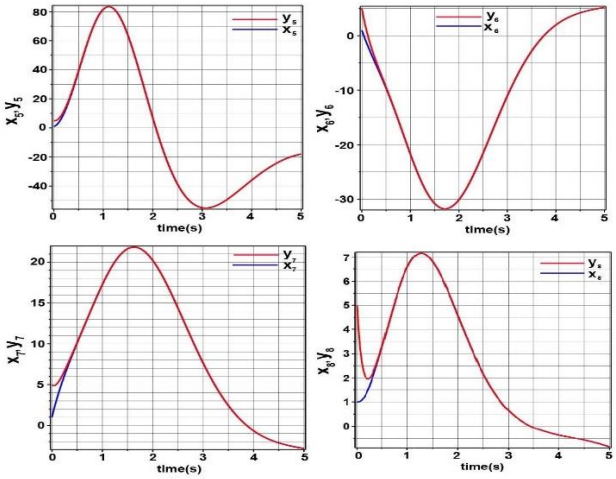

Figure 4: Synchronization of the states $x_5 - y_5, x_6 - y_6, x_7 - y_7, x_8 - y_8$ of the chaotic systems.

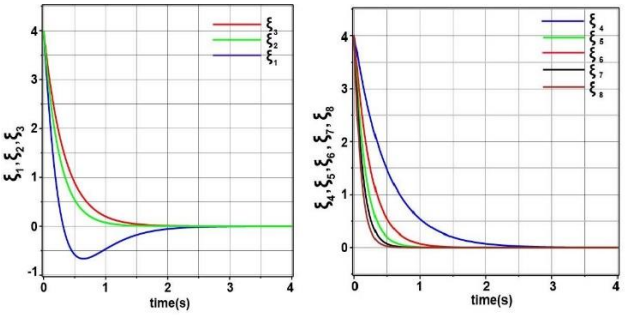

Figure 5: Time-history of the synchronization errors.

$$x_1(0) = x_2(0) = x_3(0) = x_4(0) = 1,$$
$$x_5(0) = x_6(0) = x_7(0) = x_8(0) = 1.$$

The initial value of the parameter estimate is taken as $R(0) = 59$.

Figure 2 shows the time history of the controlled novel chaotic system. It is proven that the controlled system (6) is globally exponentially stable when the adaptive control law (7) and the parameter update law (12) are implemented.

For numerical simulations, the bifurcation parameter value of the novel drive system (3) and the novel response system (13) is taken as in the chaotic case, viz. $R = 58$. We take the gain constants as $k_1 = 3$, $k_2 = 3$, $k_3 = 4$, $k_4 = 2$, $k_5 = 4$, $k_6 = 6$, $k_7 = 8$, and $k_8 = 10$.

The initial conditions of the drive system (3) are taken as:

$$x_1(0) = x_2(0) = x_3(0) = x_4(0) = 1,$$
$$x_5(0) = x_6(0) = x_7(0) = x_8(0) = 1$$

The initial values of the response system (13) are chosen as:

$$y_1(0) = y_2(0) = y_3(0) = y_4(0) = 5,$$
$$y_5(0) = y_6(0) = y_7(0) = y_8(0) = 5$$

The initial condition of the bifurcation parameter estimate is taken as $R(0) = 60$.

The timing diagrams of $x_1 - y_1, x_2 - y_2, x_3 - y_3, x_4 - y_4$, $x_5 - y_5, x_6 - y_6, x_7 - y_7, x_8 - y_8$ are shown in Figure 3 and 4. Figure 3 and 4 describe the complete synchronization of the

identical novel chaotic systems (3) and (13). Figure 5 shows the convergence of the synchronization errors $\xi_1, \xi_2, \xi_3, \xi_4, \xi_5, \xi_6, \xi_7, \xi_8$ to zero exponentially with time.

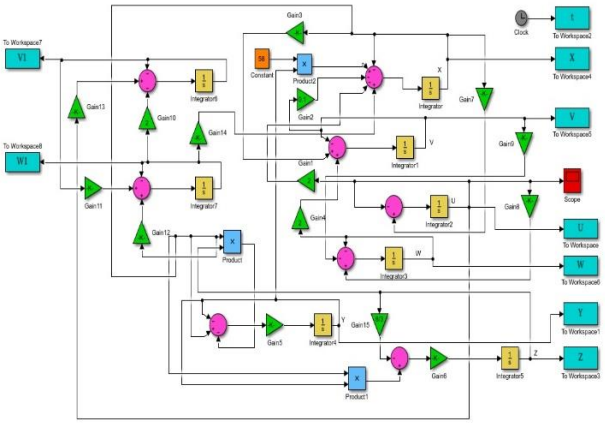

Figure 6: Matlab-Simulink model for equations (3). The simulation data is displayed using the To Workspace blocks.

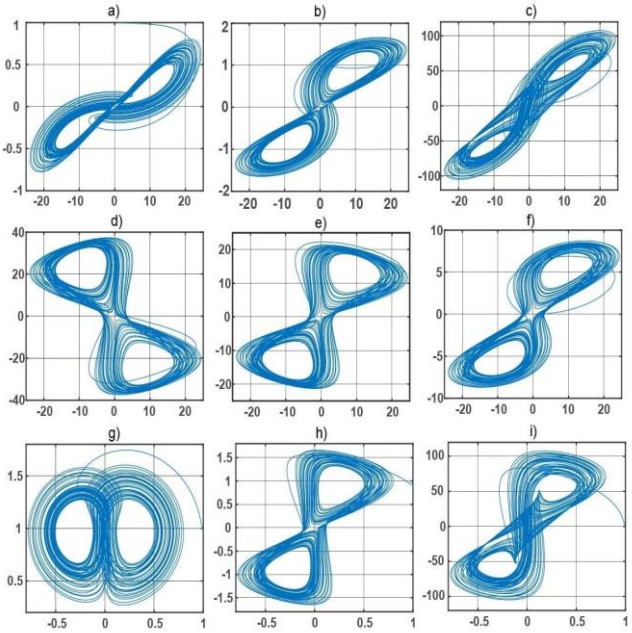

Figure 7: The phase portraits in the planes a) x_1x_2, b) x_1x_4, c) x_1x_5, d) x_1x_6 e) x_1x_7, f) x_1x_8, g) x_2x_3, h) x_2x_4, i) x_2x_5.

VII. MATLAB-SIMULINK MODEL

The system of equations (3) was numerically solved using a model developed within Matlab-Simulink environment. This model consists of interconnected blocks for amplification, summation, subtraction, multiplication, integration, and signal recording. Figure 6 shows a diagram of the Matlab-Simulink model, while Figures 7 and 8 depict the results of the simulation for the parameter $R = 58$. The phase portraits in Figures 7 and 8 show the complexity of the trajectories, which is a distinctive feature of strange attractors.

It is worth noting that directly implementing equations (3) in an electronic circuit poses certain difficulty. The dynamic variables x_1, x_5, x_6, x_7, x_8 in (3) occupy a wide dynamic range with values that go beyond typical power supply limitations. In practical electronic circuits, operational amplifiers typically operate within a voltage range of -15 V to +15 V. This issue can be mitigated through a simple transformation of variables in the dynamic system [4]. For our case, we need to rescale the following variables: $x_1 = 10X_1, x_5 = 20X_5, x_6 = 10X_6, x_7 = 10X_7, x_8 = 5X_8$.

The remaining variables are simply redesignated as $x_2 = X_2, x_3 = X_3, x_4 = X_4$. Consequently, equations (3) are transformed using this scaling to the following form:

$$\begin{cases} \dot{X}_1 = -X_1 + 5.8X_2 - 0.2X_4 - 0.2X_5 + 0.03X_8 \\ \dot{X}_2 = -0.1X_2 + X_1 - X_1X_3 \\ \dot{X}_3 = -\dfrac{8}{30}X_3 + X_1X_2 \\ \dot{X}_4 = -X_4 + X_1 \\ \dot{X}_5 = -X_5 + 4.12X_1 + X_6 \\ \dot{X}_6 = -X_6 - 2.465X_4 - 0.2X_5 \\ \dot{X}_7 = -X_7 + 2.84X_4 - X_8 \\ \dot{X}_8 = -X_8 + 0.94X_1 + 0.2X_7 \end{cases} \tag{20}$$

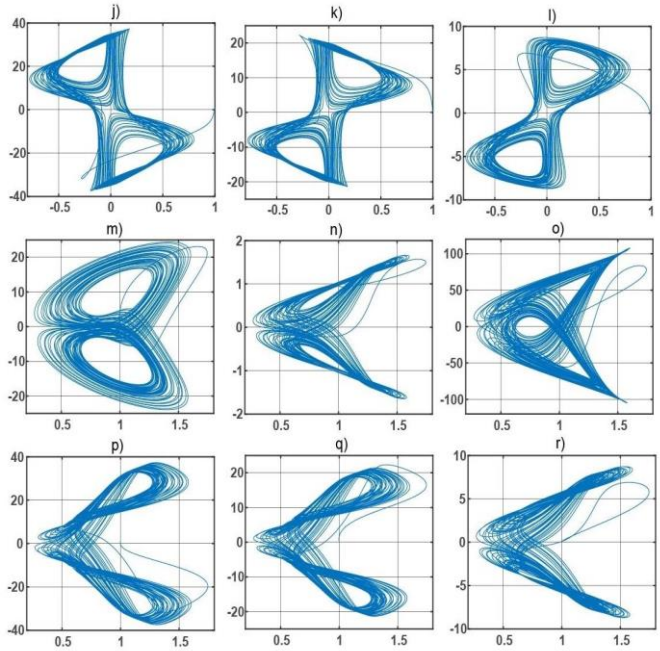

Figure 8: The phase portraits in the planes j) x_2x_6, k) x_2x_7, l) x_2x_8, m) x_3x_1, n) x_3x_4, o) x_3x_5, p) x_3x_6, q) x_3x_7, r) x_3x_8.

Note that the two systems (3) and (20) are equivalent, as the linear transformation only changes the variables but not the physical properties of the nonlinear system. The chaotic solutions of the transformed equations (20), achieved using the Matlab-Simulink model, are shown in Figures 9 and 10. It is evident that the range of values of the dynamic variables has significantly decreased in comparison to the values in Figures 7 and 8. This reduction makes it possible to implement electronic circuits using operational amplifiers that operate within the conventional voltage range of -15 V to +15 V.

VIII. LABVIEW MODEL

It is interesting to model nonlinear dynamic systems using different software environments as it allows for the

demonstration of various informational properties of chaotic oscillations.

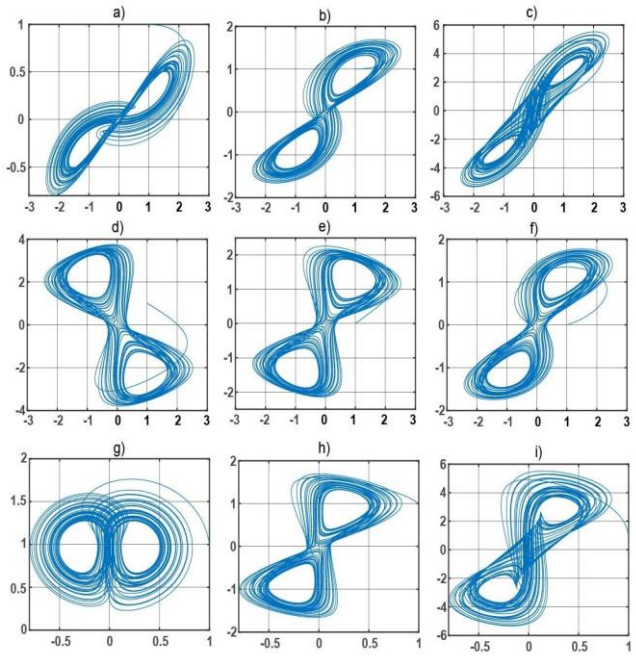

Figure 9: The phase portraits in the planes a) X_1X_2, b) X_1X_4, c) X_1X_5, d) X_1X_6, e) X_1X_7, f) X_1X_8, g) X_2X_3, h) X_2X_4, i) X_2X_5.

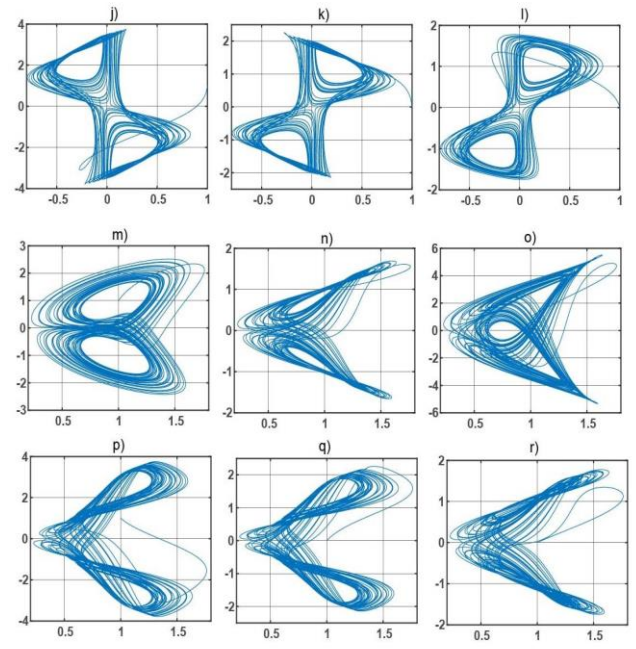

Figure 10: The phase portraits in the planes j) X_2X_6, k) X_2X_7, l) X_2X_8, m) X_3X_1, n) X_3X_4, o) X_3X_5, p) X_3X_6, q) X_3X_7, r) X_3X_8.

To simulate and showcase the results of the chaotic system (20), we utilized the LabView software environment. LabView, a graphical software platform, is widely used for engineering applications [22]. A visual platform has been created for the development of algorithms in LabView. Figure 11 displays a block diagram of the chaotic system (20) created using the Control & Simulation toolbox in LabView. As shown in Figure 11, various operations such as addition, multiplication, multiplication on a fixed number, and integration were utilized to model differential equations (20). Figure 12 showcases the programming interface that illustrates the information modeling properties in the form of phase portraits in the planes such as,

$$X_1X_2, X_1X_4, X_1X_7, X_2X_3, X_2X_5, X_2X_8, X_3X_1, X_3X_5, X_3X_7$$

for the initial conditions

$$X_1(0) = X_2(0) = X_3(0) = X_4(0) = 1,$$

$$X_5(0) = X_6(0) = X_7(0) = X_8(0) = 1.$$

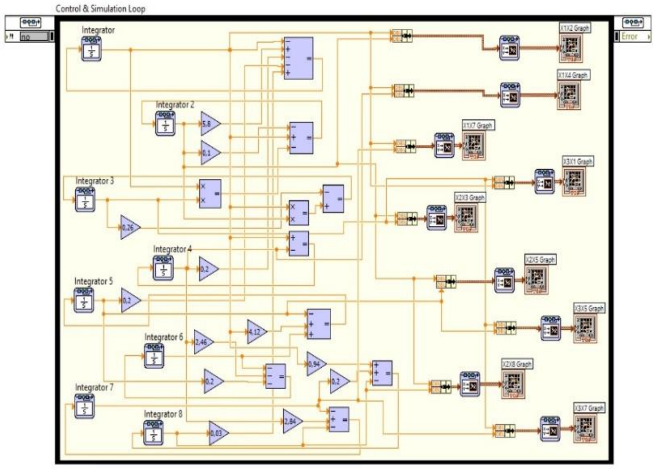

Figure 11: Block diagram implementing chaotic system (6) in LabView.

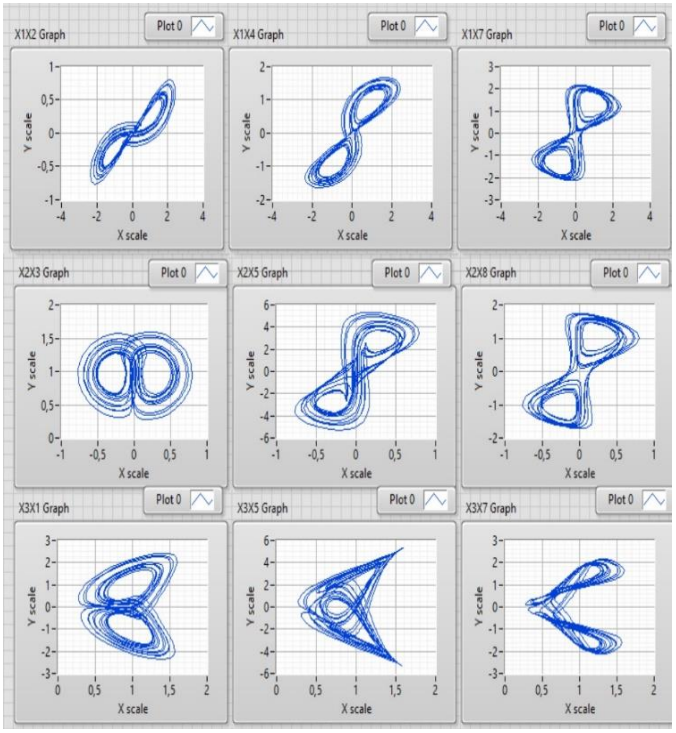

Figure 12: Phase portraits are simulated in LabView.

By comparing the phase portraits in Figures 9 and 10 with Figure 12, it can be observed that the results of modeling the chaotic system (20) in Matlab-Simulink and LabView are consistent.

IX. CIRCUIT SIMULATION

The implementation of chaotic systems in circuits is crucial for various engineering applications, suc as the secure communications and the random bit generation.

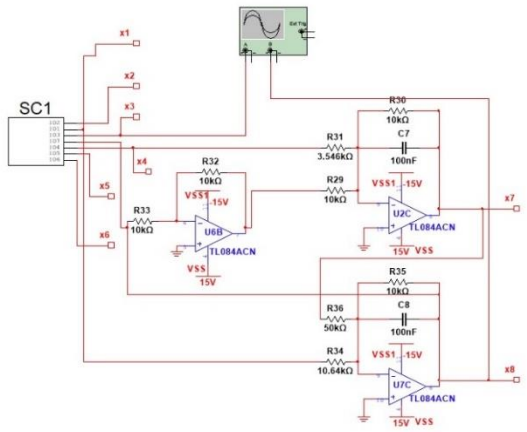

Figure 13: Electronic circuit of the generator of chaotic oscillations based on the system of equations (23).

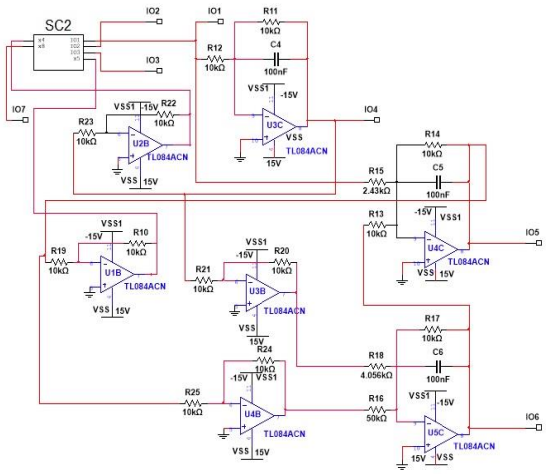

Figure 14: Electronic circuit of the subsystem SC1.

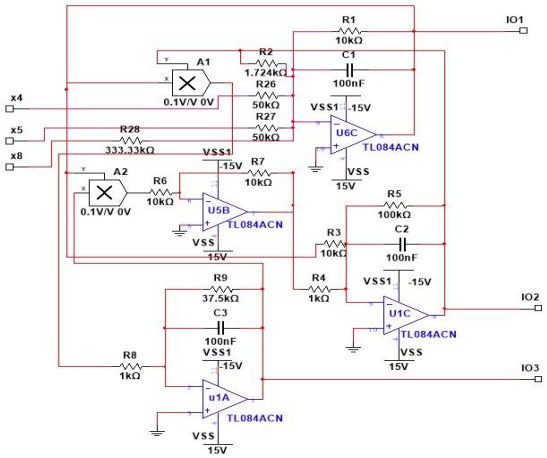

Figure 15: Electronic circuit of the subsystem SC2.

To implement the dynamic system of equations (20) in a circuit, eight operational amplifiers are used to perform the signal integration function. The dynamic system variables (20) are represented by electrical signals that correspond to the instantaneous voltage values on capacitors $C_1, C_2, C_3, C_4, C_5, C_6, C_7, C_8$, which are denoted by $U_1(\tau), U_2(\tau), U_3(\tau), U_4(\tau), U_5(\tau), U_6(\tau), U_7(\tau), U_8(\tau)$.

The electrical analogue of the system (20) in accordance with the laws of Kirchhoff for electrical circuits, takes the following form:

$$\begin{cases} C_1\dfrac{dU_1}{d\tau} = -\dfrac{U_1}{R_{11}} + \dfrac{U_2}{R_{12}} - \dfrac{U_4}{R_{13}} - \dfrac{U_5}{R_{14}} + \dfrac{U_8}{R_{15}} \\ C_2\dfrac{dU_2}{d\tau} = -\dfrac{U_2}{R_{21}} + \dfrac{U_1}{R_{22}} - \dfrac{U_1U_3}{R_{23}K} \\ C_3\dfrac{dU_3}{d\tau} = -\dfrac{U_3}{R_{31}} + \dfrac{U_1U_2}{R_{32}K} \\ C_4\dfrac{dU_4}{d\tau} = -\dfrac{U_4}{R_{41}} + \dfrac{U_1}{R_{42}} \\ C_5\dfrac{dU_5}{d\tau} = -\dfrac{U_5}{R_{51}} + \dfrac{U_1}{R_{52}} + \dfrac{U_6}{R_{53}} \\ C_6\dfrac{dU_6}{d\tau} = -\dfrac{U_6}{R_{61}} - \dfrac{U_4}{R_{62}} - \dfrac{U_5}{R_{63}} \\ C_7\dfrac{dU_7}{d\tau} = -\dfrac{U_7}{R_{71}} + \dfrac{U_4}{R_{72}} - \dfrac{U_8}{R_{73}} \\ C_8\dfrac{dU_8}{d\tau} = -\dfrac{U_8}{R_{81}} + \dfrac{U_1}{R_{82}} + \dfrac{U_7}{R_{83}} \end{cases} \tag{21}$$

where R_{ij} are resistors $(i, j) = 1,2,3,4,5,6,7,8$; K is a scale coefficient for the multiplier. We choose the normalised resistor as $R_0 = 10\,\text{k}\Omega$, and the normalised capacitor as $C_0 = 100$ nF. Then the time constant is equal to $t_0 = R_0C_0 = 10^{-3}$ s. We rescale the state variables of the system (21) as follows:

$$U_1 = U_0\tilde{X}_1, U_2 = U_0\tilde{X}_2, U_3 = U_0\tilde{X}_3, U_4 = U_0\tilde{X}_4,$$
$$U_5 = U_0\tilde{X}_5, U_6 = U_0\tilde{X}_6, U_7 = U_0\tilde{X}_7, U_8 = U_0\tilde{X}_8$$

and $K = U_0K'$, $\tau = t_0t$ and equations (21) are written in a dimensionless form such as:

$$\begin{cases} \dfrac{C_1}{C_0}\dfrac{d\tilde{X}_1}{dt} = -\dfrac{R_0}{R_{11}}\tilde{X}_1 + \dfrac{R_0}{R_{12}}\tilde{X}_2 - \dfrac{R_0}{R_{13}}\tilde{X}_4 - \dfrac{R_0}{R_{14}}\tilde{X}_5 + \dfrac{R_0}{R_{15}}\tilde{X}_8 \\ \dfrac{C_2}{C_0}\dfrac{d\tilde{X}_2}{dt} = -\dfrac{R_0}{R_{21}}\tilde{X}_2 + \dfrac{R_0}{R_{22}}\tilde{X}_1 - \dfrac{R_0}{R_{23}K'}\tilde{X}_1\tilde{X}_3 \\ \dfrac{C_3}{C_0}\dfrac{d\tilde{X}_3}{dt} = -\dfrac{R_0}{R_{31}}\tilde{X}_3 + \dfrac{R_0}{R_{32}K'}\tilde{X}_1\tilde{X}_2 \\ \dfrac{C_4}{C_0}\dfrac{d\tilde{X}_4}{dt} = -\dfrac{R_0}{R_{41}}\tilde{X}_4 + \dfrac{R_0}{R_{42}}\tilde{X}_1 \\ \dfrac{C_5}{C_0}\dfrac{d\tilde{X}_5}{dt} = -\dfrac{R_0}{R_{51}}\tilde{X}_5 + \dfrac{R_0}{R_{52}}\tilde{X}_1 + \dfrac{R_0}{R_{53}}\tilde{X}_6 \\ \dfrac{C_6}{C_0}\dfrac{d\tilde{X}_6}{dt} = -\dfrac{R_0}{R_{61}}\tilde{X}_6 - \dfrac{R_0}{R_{62}}\tilde{X}_4 - \dfrac{R_0}{R_{63}}\tilde{X}_5 \\ \dfrac{C_7}{C_0}\dfrac{d\tilde{X}_7}{dt} = -\dfrac{R_0}{R_{71}}\tilde{X}_7 + \dfrac{R_0}{R_{72}}\tilde{X}_4 - \dfrac{R_0}{R_{73}}\tilde{X}_8 \\ \dfrac{C_8}{C_0}\dfrac{d\tilde{X}_8}{dt} = -\dfrac{R_0}{R_{81}}\tilde{X}_8 + \dfrac{R_0}{R_{82}}\tilde{X}_1 + \dfrac{R_0}{R_{83}}\tilde{X}_7 \end{cases} \tag{22}$$

Substituting $R_0 = 10\,\text{k}\Omega$,
$C_1 = C_2 = C_3 = C_4 = C_5 = C_6 = C_7 = C_8 = C_0 = 100\,\text{nF}$

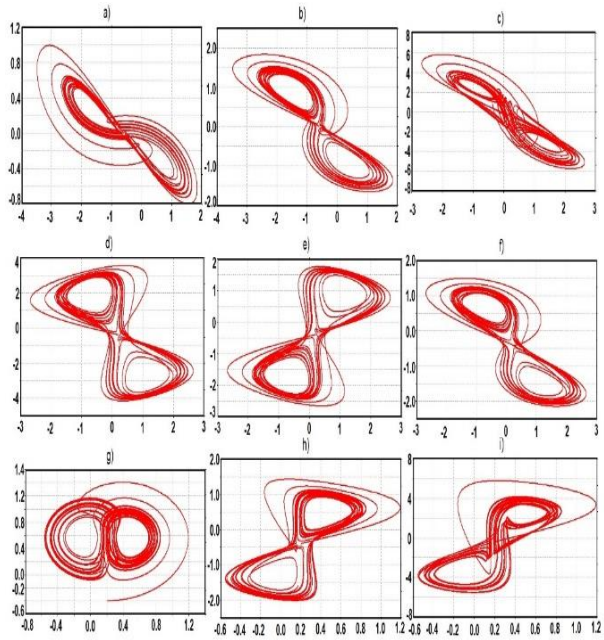

Figure 16: Chaotic phase trajectories displayed in Multisim oscilloscopes: a) $\tilde{X}_1\tilde{X}_2$, b) $\tilde{X}_1\tilde{X}_4$, c) $\tilde{X}_1\tilde{X}_5$, d) $\tilde{X}_1\tilde{X}_6$, e) $\tilde{X}_1\tilde{X}_7$, f) $\tilde{X}_1\tilde{X}_8$, g) $\tilde{X}_2\tilde{X}_3$, h) $\tilde{X}_2\tilde{X}_4$, i) $\tilde{X}_2\tilde{X}_5$.

and $K' = 10$ into (22). Comparing the numerical values before the output voltages of the system (22) and (20), the value of electronic circuit resistors is obtained:

$$\begin{cases} \dfrac{d\tilde{X}_1}{dt} = -\dfrac{10k}{10k}\tilde{X}_1 + \dfrac{10k}{1.724k}\tilde{X}_2 - \dfrac{10k}{50k}\tilde{X}_4 - \dfrac{10k}{50k}\tilde{X}_5 + \dfrac{10k}{333.33k}\tilde{X}_8 \\ \dfrac{d\tilde{X}_2}{dt} = -\dfrac{10k}{100k}\tilde{X}_2 + \dfrac{10k}{10k}\tilde{X}_1 - \dfrac{10k}{1k\cdot 10}\tilde{X}_1\tilde{X}_3 \\ \dfrac{d\tilde{X}_3}{dt} = -\dfrac{10k}{37.5k}\tilde{X}_3 + \dfrac{10k}{1k\cdot 10}\tilde{X}_1\tilde{X}_2 \\ \dfrac{d\tilde{X}_4}{dt} = -\dfrac{10k}{10k}\tilde{X}_4 + \dfrac{10k}{10k}\tilde{X}_1 \\ \dfrac{d\tilde{X}_5}{dt} = -\dfrac{10k}{10k}\tilde{X}_5 + \dfrac{10k}{2.43k}\tilde{X}_1 + \dfrac{10k}{10k}\tilde{X}_6 \\ \dfrac{d\tilde{X}_6}{dt} = -\dfrac{10k}{10k}\tilde{X}_6 - \dfrac{10k}{4.056k}\tilde{X}_4 - \dfrac{10k}{50k}\tilde{X}_5 \\ \dfrac{d\tilde{X}_7}{dt} = -\dfrac{10k}{10k}\tilde{X}_7 + \dfrac{10k}{3.546k}\tilde{X}_4 - \dfrac{10k}{10k}\tilde{X}_8 \\ \dfrac{d\tilde{X}_8}{dt} = -\dfrac{10k}{10k}\tilde{X}_8 + \dfrac{10k}{10.64k}\tilde{X}_1 + \dfrac{10k}{50k}\tilde{X}_7 \end{cases} \quad (23)$$

The Multisim software environment is used to design a circuit for generating chaotic oscillations in the system described by equations (23). In this process, operational amplifiers are used as integrators. The circuit is designed using standard methods for integrating, summing, and inverting signals. Figure 13 shows the analog circuit of the system (23), with the initial six equations conveniently implemented in a subsystem labeled as SC1. Figure 14 shows the electronic circuit of the SCI subsystem, which also includes another subsystem, SC2, representing the first three equations of system (23) (similar to Lorentz equations). The electronic circuit of subsystem SC2 is displayed in Figure 15.

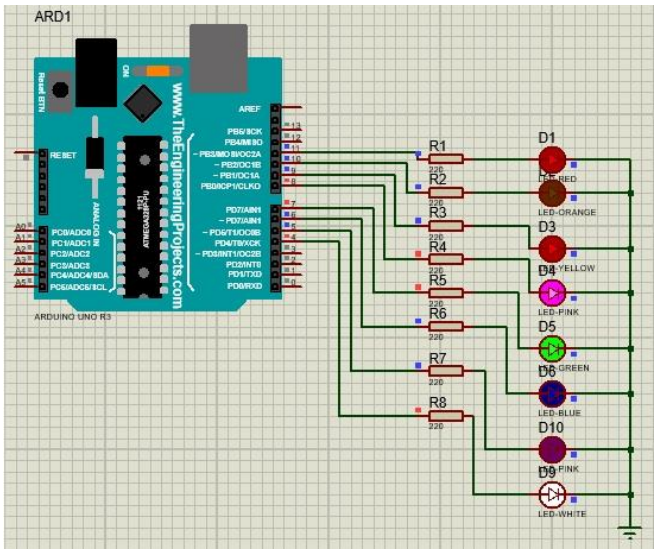

Figure 17: Microcontroller circuit of the 8D chaotic oscillator depicted in Proteus 8.

The circuits illustrated in Figures 13, 14, and 15 are based on operational amplifiers TL084ACN and analogue multipliers A1 and A2. The signal outputs correspond to the terminals labeled in the circuit diagram. By connecting a dual-channel oscilloscope to different outputs, various phase portraits can be obtained in the Multisim environment, as shown in Figure 16. The results obtained from Multisim outputs are similar to those obtained from Matlab-Simulink in Figures 9 and 10 and LabView in Figure 12.

X. IMPLEMENTATION OF THE NEW 8D CHAOTIC SYSTEM ON AN ARDUINO UNO BOARD

To implement the new developed 8D chaotic system on the Arduino Uno board, we utilize the Proteus 8 environment. We connect a matrix of eight LEDs to the digital pins (D4-D11) of the microcontroller using eight 220 Ohm resistors (as shown in Figure 17). The programme code (accessible at the provided link, https://wokwi.com/projects/362267327996080129) uses the Euler method to numerically solve the state variables of the 8D dynamic system. The program code is compiled in the Arduino IDE software and a hex.file is generated for programming the Arduino Uno R3 microcontroller in the Proteus 8 environment. It is noteworthy to mention that the brightness of the LEDs varies depending on the output voltage in each channel.

XI. CONCLUSION

In summary, this study provides a comprehensive analysis of a new 8D chaotic system, inclusive of its fundamental properties and phase portraits. Furthermore, an adaptive controller was developed to stabilize the system with unknown parameters and to synchronize two identical chaotic systems. Numerical simulations using Matlab-Simulink and LabView models were carried out to investigate the dynamics of the system. The simulations revealed complex chaotic oscillations in the system, as demonstrated by the phase portraits. In addition, an electronic circuit for a chaos generator was designed using operational amplifiers and tested in the Multisim environment. The findings of this study hold significant

potential for applications in various fields, including secure communications and random bit generation. Today's digital technologies can benefit greatly from the use of an 8D chaotic generator, as demonstrated by the implementation of an Arduino. Integrating chaos generators in electronic devices could potentially pave the way for the development of more secure communication systems that are challenging to intercept or decode.

ACKNOWLEDGMENT

The authors are grateful to anonymous reviewers for their interest in this manuscript.

REFERENCES

[1] Fei Yu, Zinan Zhang, Li Li, Hui Shen, et al. "Secure Communication Scheme Based on a New 5D Multistable Four-Wing Memristive Hyperchaotic System with Disturbance Inputs," *Complexity*, vol. 2020, pp. 1-16, 2020.

[2] A. Ouannas, et al., "A Novel Secure Communications Scheme Based on Chaotic Modulation, Recursive Encryption and Chaotic Masking," *Alexandria Engineering Journal*, vol. 60, no. 1, pp. 1873-1884, 2020.

[3] E. N. Lorenz, "Deterministic Non-Periodic Flow," *Journal of the Atmospheric Sciences*, vol. 20, pp. 130-142, 1963.

[4] K. M. Cuomo, A. V. Oppenheim, "Circuit Implementation of Synchronized Chaos with Applications to Communications," *Physical Review Letters*, vol. 71, no. 1, pp. 65-68, Aug. 1993.

[5] A. Sambas, W. S. M. Sanjaya and M Mamat, "Design and Analysis Bidirectional Chaotic Synchronization of Rossler Circuit and Its Application for Secure Communication," *Applied Mathematical Sciences*, vol. 7, pp. 11-21, 2013.

[6] K. M. Ibrahim, R. K. Jamal and F. H. Ali, "Chaotic Behavior of the Rossler Model and Its Analysis by Using Bifurcations of Limit Cycles and Chaotic Attractors," *Journal of Physics: Conference Series*, vol. 1003, no. 1, Article no. 012099, May 2018.

[7] Y. Y. Hou, Cheng-Shun Fang, Chang-Hua Lien, Sundarapandian Vaidyanathan, et al., "Rikitake Dynamo System, Its Circuit Simulation and Chaotic Synchronization via Quasi-Sliding Mode Control," *TELKOMNIKA Telecommunication, Computing, Electronics, and Control*, vol. 19, no. 4, pp. 1428-1438, 2021.

[8] F. Hannachi, "Analysis, Dynamics and Adaptive Control Synchronization of a Novel Chaotic 3D System," *SN Applied Sciences*, vol. 1, no. 2, Article no. 158, 2019.

[9] A. Sambas, et al., "Dynamics, Circuit Design and Fractional-Order Form of a Modified Rucklidge Chaotic System," *Journal of Physics: Conference Series*, vol. 1090, no. 1, Article no. 012038, Sept. 2018.

[10] F. Q. Wang, et al., "Hyperchaos Evolved from the Liu Chaotic System," *Chinese Physics B*, vol. 15, no. 5, pp. 963-968, May 2006.

[11] M. W. Luo, et al., "Circuitry Implementation of a Novel Four-Dimensional Nonautonomous Hyperchaotic Liu System and Its Experimental Studies on Synchronization Control," *Chinese Physics B*, vol. 18, no. 6, pp. 2168-2175, Jun. 2009.

[12] J. Lu, et al., "The Compound Structure of a New Chaotic Attractor," *Chaos, Solitons, and Fractals*, vol. 14, no. 5, pp. 669-672, Sept. 2002.

[13] L. Xiong, et al., "Dynamical Analysis, Synchronization, Circuit Design, and Secure Communication of a Novel Hyperchaotic System," *Complexity*, vol. 2017, Article no. 4962739, 2017.

[14] L. Xiong, et al., "Circuit Implementation and Antisynchronization of an Improved Lorenz Chaotic System," *Shock and Vibration*, vol. 2016, Article no. 1617570, 2016.

[15] S. Vaidyanathan, et al., "A 5D Hyperchaotic Rikitake Dynamo System with Hidden Attractors," *The European Physical Journal Special Topics*, vol. 224, pp. 1575-1592, 2015.

[16] S. Vaidyanathan, et al., "A 5D Multi-Stable Hyperchaotic Two-Disk Dynamo System with no Equilibrium Point: Circuit Design, FPGA Realization and Applications to TRNGs and Image Encryption," *IEEE Access*, vol. 9, pp. 81352-81369, 2021.

[17] M. I. Kopp, A. V. Tur, V. V. Yanovsky, "Magnetic convection in a nonuniformly rotating electrically conductive medium in an external spiral magnetic field*," Fluid Dyn. Res*., vol. 53, 015509, 2021.

[18] M. I. Kopp, A. V. Tur, and V. V. Yanovsky, "Magnetic Convection in a Nonuniformly Rotating Electroconducting Medium," *J. Exp. Theor. Phys.*, vol. 127, pp. 1173-1196, 2018.

[19] G. Benettin, L. Galgani, A. Giorgilli, and J. M. Strelcyn, "Lyapunov characteristic exponents for smooth dynamical systems and for Hamiltonian systems: A method for computing all of them," *Meccanica*, vol. 15, pp. 9-30, 1980.

[20] A. Wolf, J. B. Swift, H. L. Swinney, and J. A. Vastano, "Determining Lyapunov Exponents from a Time Series," *Phys. D: Nonlinear Phenom.*, vol. 16, pp. 285-317, 1985.

[21] M. Sandri, "Numerical Calculation of Lyapunov Exponents," *Mathematica J.*, vol. 6, pp. 78-84, 1996.

[22] R. W. Larsen, *LabVIEW for Engineers*. Upper Saddle River: Prentice Hall, 2011.